

This is the author's peer reviewed, accepted manuscript. However, the online version of record will be different from this version once it has been copyedited and typeset.

PLEASE CITE THIS ARTICLE AS DOI: 10.1063/1.50046904

Spin echo from erbium implanted silicon

Mark A. Hughes,^{*1} Naitik A. Panjwani,^{2,3} Matias Urdampilleta,^{2,4} Kevin P. Homewood,^{5,6}
Ben Murdin,⁵ and J. David Carey^{5,7}

¹Materials and Physics Research Group, School of Science, Engineering and Environment,
University of Salford, Salford, M5 4WT, UK

²University College London, London Centre for Nanotechnology, Gower Place, WC1E 6BT,
London, UK

³Berlin Joint EPR Lab, Fachbereich Physik, Freie Universität Berlin, D-14195 Berlin,
Germany

⁴Institut Néel-CNRS-UJF-INPG, UPR2940 25 rue des Martyrs BP 166, 38042 Grenoble
cedex 9, France

⁵Advanced Technology Institute, Faculty of Engineering and Physical Sciences, University of
Surrey, Guildford, GU2 7XH, UK

⁶School of Materials Science and Engineering, Hubei University, Wuhan, 430062, Peoples
Republic of China

⁷Department of Electrical and Electronic Engineering, University of Surrey, Guildford, GU2
7XH, UK

*Email: *m.a.hughes@salford.ac.uk*

This is the author's peer reviewed, accepted manuscript. However, the online version of record will be different from this version once it has been copyedited and typeset.

PLEASE CITE THIS ARTICLE AS DOI: 10.1063/1.50046904

Abstract

Erbium implanted silicon as a quantum technology platform has both telecommunications and integrated circuit (IC) processing compatibility. In Si implanted with Er to a concentration of $3 \times 10^{17} \text{ cm}^{-3}$ and O to a concentration of 10^{20} cm^{-3} , the electron spin coherence time, T_2 , and the spin-lattice relaxation time, T_1 , were measured to be $7.5 \mu\text{s}$ and $\sim 1 \text{ ms}$, respectively, at 5 K. The spin echo decay profile displayed strong modulation which was consistent with the super-hyperfine interaction between Er^{3+} and a spin bath of ^{29}Si nuclei. The calculated spectral diffusion time was similar to the measured T_2 , which indicated that T_2 was limited by spectral diffusion due to T_1 -induced flips of neighbouring Er^{3+} spins. The origin of the echo is an Er centre surrounded by six O atoms with monoclinic C_{1h} site symmetry.

This is the author's peer reviewed, accepted manuscript. However, the online version of record will be different from this version once it has been copyedited and typeset.

PLEASE CITE THIS ARTICLE AS DOI: 10.1063/1.50046904

The optical fibre telecommunications network makes telecoms wavelength photons at 1.5 μm by far the best candidate for transferring quantum information over distance. Er^{3+} intra 4f shell transitions can be optically addressed at telecommunications C band wavelengths which would allow transfer of quantum information over distance. The use of rare earth (RE) ions is well suited to overcome a paradox of quantum technology (QT) platform requirements: sufficient decoupling from the environment to avoid decoherence, but a strong enough interaction with the environment to allow addressing, readout and gating. The advantage of RE ions arises as they possess a partially filled 4f shell which is shielded from the environment by the outer 5s and 5p shells, leading to extraordinary coherence times of 6 hours for optically detected nuclear spin¹ and 4.4 ms for optical transitions;² however, even with their atomic scale shielding, long lived entanglement between RE dopants in a solid matrix has been observed,^{3, 4} and entanglement between internal degrees of freedom of single RE ions, with a less than half filled 4f shell, can still exist up to thousands of Kelvin, making this one of the most stable known entanglements.⁵

Architectures based on Si offer considerable promise for developing a practical and scalable pathway for quantum computer fabrication, and features can be patterned in Si on the scale required for many quantum device architectures. Ion implantation of Si is a well understood technology in IC fabrication, and commercial adoption of new technologies tend to favour those based on established fabrication platforms and techniques. Recently, increases in coherence times by several orders of magnitude have been demonstrated in donor impurities in silicon by using isotopically pure ^{28}Si .⁶ However, these donor impurities do not interact with light at telecommunications wavelengths, which is critical for many quantum communication schemes. A possible alternative is the T-centre in Si, thought to be composed of two carbon atoms, which displays spin-selective bound exciton optical transitions at 1326 nm.⁷ Given expected improvements in T_2 by using ^{28}Si , optimising processing for the

This is the author's peer reviewed, accepted manuscript. However, the online version of record will be different from this version once it has been copyedited and typeset.

PLEASE CITE THIS ARTICLE AS DOI: 10.1063/1.50046904

appropriate Er-related centre⁸ and reducing Er concentration, Er implanted Si is potentially the only known QT platform with telecommunications C band addressability, long T_2 and IC tooling compatibility. The spin state of a single Er ion implanted into a silicon single electron transistor has been optically addressed and electrically readout,⁹ whereas, the spin state of a single Er ion in Y_2SiO_5 , coupled to a silicon nanophotonic cavity, can be readout optically with a single shot.¹⁰ This demonstrates that Er implantation is compatible with single electron transistors, which are used in the readout of quantum dot qubits.¹¹ Here we report spin echo measurements of Er implanted Si.

A sample, with an Er concentration of $3 \times 10^{17} \text{ cm}^{-3}$ and an O concentration of 10^{20} cm^{-3} , was prepared by implanting Er and O ions into a $\langle 100 \rangle$ oriented $8000 \pm 500 \Omega \text{ cm}$ Si wafer. The sample was then annealed at 750°C for 2 min to recrystallize the amorphized region. O and Er ions were implanted at a range of energies to give a flat concentration profile down to a depth of around $1.5 \mu\text{m}$, see supplementary Fig. S1. The uncertainty in the Er dose, the accuracy of the implant simulation, and diffusion after annealing¹² contribute to an uncertainty in the Er concentration of $\pm 10\%$. Isotope specific implantation was used so that only the zero nuclear spin ^{166}Er was implanted.

CW and pulsed ESR measurements were performed in a Bruker E580 ESR spectrometer. All ESR measurements were recorded with the magnetic field, B_0 , parallel to the [001] direction of the wafer with an uncertainty of $\pm 5^\circ$. For pulsed measurements the Q factor was detuned to ~ 100 , the π pulse width and repetition time were 32 ns, and 4.5 ms, respectively. Phase cycling was used in pulsed measurements, but this failed to remove an off-resonance echo signal which was also present in empty tube measurements. This off-resonance echo signal was subtracted during analysis. All CW ESR measurements were made at 10 K, all pulsed measurements at 5 K, and the microwave frequency was 9.61 GHz.

This is the author's peer reviewed, accepted manuscript. However, the online version of record will be different from this version once it has been copyedited and typeset.

PLEASE CITE THIS ARTICLE AS DOI: 10.1063/1.50046904

When implanted into Si, Er exists in its usual 3+ oxidation state.¹³ Oxygen was co-implanted to a concentration of 10^{20} cm⁻³ and is required to generate narrow Er-related ESR¹⁴ and photoluminescence (PL)¹⁵ lines by the creation of various O coordinated Er (Er-O) centres. Previous measurements of the angular dependence of the Er-related ESR lines in Er implanted Si have identified a number of different Er-O ESR centres: three monoclinic centres labelled OEr-1, OEr-1' and OEr-3, and three trigonal centres labelled OEr-2, OEr-2' and OEr-4.^{14, 16-18} Also, Zeeman measurements of molecular beam epitaxy (MBE) grown Er doped Si have identified an orthorhombic Er-O centre, labelled Er-1,¹⁹ which, possibly because of a long T_1 , is not ESR active.²⁰ We have not yet linked any of the ESR centres to the numerous PL lines observed in Er implanted Si; however, the Zeeman ground state of the Er-1 centre can be readily populated by 1.5 μ m laser radiation,²⁰ which should also be feasible in the ESR centres.

The principal g values of these centres are given in Table I. For all ESR centres the g_y -axis is parallel to a [1 1 0] direction and the mutually perpendicular g_x - and g_z -axis lie in the (1 1 0) plane with the g_x -axis tilted away from [0 0 1] by an angle τ .

This is the author's peer reviewed, accepted manuscript. However, the online version of record will be different from this version once it has been copyedited and typeset.

PLEASE CITE THIS ARTICLE AS DOI: 10.1063/1.50046904

Table I The principal g values and tilt angles, τ , of Er doped Si determined by ESR and Zeeman measurements.

Centre	Symmetry	g_x	g_y	g_z	τ	Ref.
ESR						
OEr-1	Monoclinic C_{1h}	0.8	5.45	12.6	57.30°	¹⁴
OEr-1'	Monoclinic C_{1h}	0.8	5.45	12.55	56.90°	¹⁴
OEr-3	Monoclinic C_{1h}	1.09	5.05	12.78	48.30°	¹⁴
OEr-4	Trigonal C_{3v}	2.0	6.23	6.23	54.74°	¹⁴
OEr-2	Trigonal C_{3v}	0.45	3.46	3.22	55.90°	¹⁴
OEr-2'	Trigonal C_{3v}	0.69	3.24	3.24	54.74°	¹⁴
Zeeman						
Er-1	Orthorhombic C_{2v}	~ 0	~ 0	18.4	45°	^{19, 21}

Fig. 1a shows the measured and simulated CW ESR, and the field dependent echo. There are two main resonances at 867 and 934 G, respectively, with weaker resonances at 892 and 964 G. We simulated the ESR spectra of each centre with their g -values and tilt angle using EASYSYSPIN;²² the code can be found in the associated dataset. Only the OEr-3 centre can explain the observed resonances. We simulated varying the rotation angle (angle between [001] and B_0 in the $(1\bar{1}0)$ plane) and found the closest match between simulated and observed ESR spectra with a rotation angle of 5.2° . The discrepancy between the simulated and measured spectra should be due to some small differences in the g -values and tilt angle of our $3 \times 10^{17} \text{ cm}^{-3}$ Er sample, and the 10^{19} cm^{-3} Er sample in ref. 14. All of the measured ESR resonances are visible in the echo spectrum, showing that the echo originates from the Er ESR centres. The Er-related ESR lines have been attributed to an Er^{3+} centre based on similar

g -values to Er doped Y_2O_3 , which has the same crystal structure as Er_2O_3 , and EXAFS measurements of Er and O implanted Si which found a similar Er-O bond length to that in Er_2O_3 .^{14, 18} A spin echo signal was also present off-resonance, and was also present in empty tube measurements, we therefore treated the off-resonance echo as a background and subtracted it, as illustrated in supplementary Fig. S2.

Fig. 1b shows the echo intensity as a function of B_0 for various t_{12} between 0.14 and 2.24 μs . The on-resonance echo signal disappears below the detection limit then reappears with increasing t_{12} , indicating the presence of strong electron spin echo envelope modulation (ESEEM).

In Fig. 2a we show the echo decay profile at a fixed B_0 of 867 G, corresponding to the OEr-3 centre. The background echo signal was subtracted as shown in supplementary Fig. S3 to give a recovered resonance echo decay. As can be seen from Fig. 1a, a subtraction of the echo signal at 850 G from that at 867 G, should leave only the echo component attributable to implanted Er. The echo decay in Fig. 2a displays strong superimposed oscillations from the ESEEM effect²³ caused by superhyperfine coupling with neighbouring nuclear spins; similar oscillations were observed in Er:CaWO₄, but were significantly weaker than those seen here.²⁴ Since the 4f wavefunction is highly localised, the superhyperfine coupling between a RE and a neighbouring nuclear spin is usually regarded as magnetic dipole-dipole only.^{25, 26} The ESEEM effect when using to a two pulse echo sequence, $V_{2p}(t_{12})$, on an isolated Er^{3+} ion (effective electron spin $S = 1/2$) in proximity to a ^{29}Si nuclei (nuclear spin $I = 1/2$) can be described as follows,²³

$$V_{2p}(t_{12}) = 1 - \frac{k}{4} \left[2 - 2 \cos(2\pi\nu_\alpha t_{12}) - 2 \cos(2\pi\nu_\beta t_{12}) + \cos(2\pi(\nu_\alpha - \nu_\beta)t_{12}) + \cos(2\pi(\nu_\alpha + \nu_\beta)t_{12}) \right], \quad (1)$$

where k is the modulation index, ν_α and ν_β are the ^{29}Si nuclear resonance frequencies for the two possible Er^{3+} electron spin orientations ($S = \pm 1/2$). The OEr-3 centre, along with the other ESR centres, are thought to be O coordinated because they are only observed when O is co-implanted to a concentration 10^{20} cm^{-3} ,²⁷ and EXAFS measurements of Er and O co-implanted Si showed that the average number of O atoms surrounding the Er atom was 5.1 ± 0.5 and the average Er–O separation was 2.26 \AA .²⁸ The strong ESEEM modulation observed in Fig. 2a contains two frequencies: $\nu_1 = 0.70 \text{ MHz}$ and $\nu_2 = 1.66 \text{ MHz}$, as shown in the FFT in Fig 2b; the nuclear spin Larmor frequency (ν_L) is 0.76 MHz for ^{29}Si . One possible origin of ν_1 and ν_2 is ^{29}Si at a single crystallographic position with $\nu_\alpha = \nu_1 \approx \nu_L$ and $\nu_\beta = \nu_2 \approx 2\nu_L$. This is unlikely because a large difference in ν_α and ν_β indicates very strong coupling, which would be expected from nuclei in the first coordination sphere, which in this case is O. Also, the large modulation index is inconsistent with the 4.67% abundance of ^{29}Si and a single crystallographic position. Another possibility is ν_1 and ν_2 originate from two crystallographic positions, one with $\nu_\alpha \approx \nu_\beta \approx \nu_1 \approx \nu_L$, the other with $\nu_\alpha \approx \nu_\beta \approx \nu_2 \approx 2\nu_L$. This is unlikely because $\nu_\alpha \approx \nu_\beta \approx \nu_L$ indicates weak coupling, which, for a single crystallographic position, is inconsistent with the large modulation index. Also, a crystallographic position with $\nu_\alpha \approx \nu_\beta \approx 2\nu_L$ indicates strong coupling, which can be discounted for the same reasons given for the first possible origin. Given the structure of the OEr-3 centre, it is more likely that the observed ESEEM is due to weak coupling to many ^{29}Si nuclei, in which case each ^{29}Si nuclei has $\nu_\alpha \approx \nu_\beta \approx \nu_L$ and $k \ll 1$; in this situation the overall decay profile is given by²⁹

$$I(t_{12}) = I_0 e^{-\left(\frac{2t_{12}}{T_2}\right)^x} \left[1 - \frac{k}{4} [3 - 4 \cos(2\pi\nu_L t_{12}) + \cos(4\pi\nu_L t_{12})] \right]. \quad (2)$$

This is the author's peer reviewed, accepted manuscript. However, the online version of record will be different from this version once it has been copyedited and typeset.

PLEASE CITE THIS ARTICLE AS DOI: 10.1063/1.50046904

The $I_0 e^{-\left(\frac{2t_{12}}{T_2}\right)^x}$ term is the empirical Mims equation,³⁰ which describes the echo decay in the absence of nuclear coupling where T_2 is the spin coherence time and x is an exponential stretch factor which is determined by spin dynamics.

In Fig. 2a, fitting to Eq. 2 was consistent with the observed echo decay profile and the FFT of the measured and fitted decay in Fig. 2b were consistent with each other and indicate that v_2 is the $2\nu_L$ component of Eq. 2. The FFT peaks are broadened by the relatively short sampling time; the larger relative Fourier amplitude of v_2 in the FFT of the measured decay is a result of the low SNR of our data and our choice of a Hanning window which has relatively poor amplitude accuracy, but good spectral resolution.³¹ When we used a flat top window, the amplitudes were much closer to the fitted FFT, but the spectral resolution was inadequate. Fitting yielded $k = 0.45$, which we expect to be composed of the overall modulation effect of many crystallographic positions with $k \ll 1$. The fit also yielded a T_2 of $7.5 \pm 3 \mu\text{s}$, which compares to $\sim 5 \mu\text{s}$ at 5 K ($\sim 50 \mu\text{s}$ at 2.5 K) for $\sim 10^{16} \text{ cm}^{-3}$ Er doped CaWO_4 ,²⁴ and $1.6 \mu\text{s}$ at 1.9 K for $\sim 2 \times 10^{18} \text{ cm}^{-3}$ Er doped Y_2SiO_5 .³² This is a promising comparison given the difficulty of removing defects after implantation that could lead to decoherence. Further optimisation of the recrystallization process, reductions in Er concentration and isotopic purification of the Si may lead to coherence times applicable to quantum communication and computation.

The saturation recovery profile shown in the inset of Fig. 2a gives a spin relaxation time, T_1 , at 5 K, of $0.98 \pm 0.2 \text{ ms}$; the background subtraction is shown in supplementary Fig. S4. Spectral diffusion often limits T_2 and can be caused by various electron³³ and nuclear³⁴ spin flip-flop process. The spectral diffusion time (T_{SD}) due to T_1 -induced flips of neighbouring Er^{3+} spins can be calculated from the Er^{3+} concentration in cm^{-3} ($[\text{Er}]$), T_1 , and effective g -factor (g_e), in this case at 867 G, using Eq. 3^{30,35}

This is the author's peer reviewed, accepted manuscript. However, the online version of record will be different from this version once it has been copyedited and typeset.

PLEASE CITE THIS ARTICLE AS DOI: 10.1063/5.0046904

$$T_{SD} = \sqrt{\frac{18\sqrt{3}}{4\pi^2} \frac{\hbar}{(g_e\beta_e)^2 [Er]} T_1} \quad (3)$$

This yields a T_{SD} of 7.11 μs (6.06 to 8.24 μs given the T_1 and Er concentration uncertainty); the similarity of this time to the fitted T_2 (7.5 μs) indicates that T_2 could be limited by spectral diffusion caused by T_1 -induced flips of neighbouring Er^{3+} spins, in this case the stretch factor x in Eq. 2 would be 2. The resolution and signal to noise in the echo decay profile in Fig. 2a is insufficient to distinguish between $x = 1$ or $x = 2$; however, because of the indication that T_2 is limited by spectral diffusion the fit was performed with x fixed to 2. With x fixed to 1, T_2 was calculated to be $10 \pm 3 \mu\text{s}$.

In summary, Er implanted Si is a promising platform for the development of QTs and is potentially highly scalable since it can utilise the silicon and ion implantation technology used in the IC industry. Er implanted Si can also exploit the atomic scale barrier to decoherence that is intrinsic to REs, and the recently developed ultra-low spin environment of isotropically purified ^{28}Si , whereas the Er component itself is compatible with telecommunications wavelength photons and could be utilised for quantum communications schemes. We report a spin coherence time of 7.5 μs at 5 K for $3 \times 10^{17} \text{ cm}^{-3}$ Er implanted Si; the spin-lattice relaxation time was ~ 1 ms. The calculated spectral diffusion time was 7.11 μs , which, because of its similarity to the measured T_2 , indicated that T_2 was limited by spectral diffusion due to T_1 -induced flips of neighbouring Er^{3+} spins. The origin of the echo is an Er centre surrounded by six O atoms with monoclinic site symmetry. The spin echo decay profile had superimposed modulations due strong superhyperfine coupling with a spin bath of ^{29}Si nuclei.

This is the author's peer reviewed, accepted manuscript. However, the online version of record will be different from this version once it has been copyedited and typeset.

PLEASE CITE THIS ARTICLE AS DOI: 10.1063/5.0046904

References

1. M. Zhong, M. P. Hedges, R. L. Ahlefeldt, J. G. Bartholomew, S. E. Beavan, S. M. Wittig, J. J. Longdell and M. J. Sellars, *Nature* **517** (7533), 177-180 (2015).
2. T. Böttger, C. W. Thiel, R. L. Cone and Y. Sun, *Phys. Rev. B* **79** (11), 115104 (2009).
3. J. Bartolomé, F. Luis and J. F. Fernández, *Molecular Magnets: Physics and Applications*. (Springer, 2013).
4. S. Ghosh, T. Rosenbaum, G. Aeppli and S. Coppersmith, *Nature* **425** (6953), 48 (2003).
5. O. Duarte, C. Castro, D. Soares-Pinto and M. Reis, *Europhysics Letters* **103** (4), 40002 (2013).
6. K. Saeedi, S. Simmons, J. Z. Salvail, P. Dluhy, H. Riemann, N. V. Abrosimov, P. Becker, H.-J. Pohl, J. J. L. Morton and M. L. W. Thewalt, *Science* **342** (6160), 830-833 (2013).
7. L. Bergeron, C. Chartrand, A. Kurkjian, K. Morse, H. Riemann, N. Abrosimov, P. Becker, H.-J. Pohl, M. Thewalt and S. Simmons, *PRX Quantum* **1** (2), 020301 (2020).
8. M. A. Hughes, M. A. Lourenço, J. D. Carey, B. Murdin and K. P. Homewood, *Opt. Express* **22**, 29292–29303 (2014).
9. C. M. Yin, M. Rancic, G. G. de Boo, N. Stavrias, J. C. McCallum, M. J. Sellars and S. Rogge, *Nature* **497** (7447), 91 (2013).
10. M. Raha, S. Chen, C. M. Phenicie, S. Ourari, A. M. Dibos and J. D. Thompson, *Nat. Commun.* **11** (1), 1605 (2020).
11. M. Veldhorst, J. C. C. Hwang, C. H. Yang, A. W. Leenstra, B. de Ronde, J. P. Dehollain, J. T. Muhonen, F. E. Hudson, K. M. Itoh, MorelloA and A. S. Dzurak, *Nat Nano* **9** (12), 981-985 (2014).
12. A. Polman, *J. Appl. Phys.* **82** (1), 1-39 (1997).
13. A. J. Kenyon, *Semicond. Sci. Technol.* **20** (12), R65 (2005).
14. J. D. Carey, R. C. Barklie, J. F. Donegan, F. Priolo, G. Franzo and S. Coffa, *Phys. Rev. B* **59** (4), 2773-2782 (1999).
15. H. Przybylinska, W. Jantsch, Y. Suprun-Belevitch, M. Stepikhova, L. Palmetshofer, G. Hendorfer, A. Kozanecki, R. J. Wilson and B. J. Sealy, *Phys. Rev. B* **54** (4), 2532-2547 (1996).
16. J. D. Carey, J. F. Donegan, R. C. Barklie, F. Priolo, G. Franzò and S. Coffa, *Appl. Phys. Lett.* **69** (25), 3854-3856 (1996).
17. J. D. Carey, R. C. Barklie, J. F. Donegan, F. Priolo, G. Franzò and S. Coffa, *J. Lumines.* **80** (1–4), 297-301 (1998).
18. J. D. Carey, *J. Phys.-Condes. Matter* **14** (36), 8537 (2002).
19. N. Q. Vinh, H. Przybylińska, Z. F. Krasil'nik and T. Gregorkiewicz, *Phys. Rev. Lett.* **90** (6), 066401 (2003).
20. M. A. Hughes, H. Li, N. Theodoropoulou and J. D. Carey, *Sci. Rep.* **9** (1), 19031 (2019).
21. N. Q. Vinh, H. Przybylińska, Z. F. Krasil'nik and T. Gregorkiewicz, *Phys. Rev. B* **70** (11), 115332 (2004).
22. S. Stoll and R. D. Britt, *PCCP Phys. Chem. Chem. Phys.* **11** (31), 6614-6625 (2009).
23. L. G. Rowan, E. L. Hahn and W. B. Mims, *Phys.Rev.* **137** (1A), A61-A71 (1965).
24. S. Bertaina, S. Gambarelli, A. Tkachuk, I. N. Kurkin, B. Malkin, A. Stepanov and B. Barbara, *Nat. Nanotechnol.* **2** (1), 39-42 (2007).
25. O. Guillot-Noël, H. Vezin, P. Goldner, F. Beaudoux, J. Vincent, J. Lejay and I. Lorgère, *Phys. Rev. B* **76** (18), 180408 (2007).
26. B. Car, L. Veissier, A. Louchet-Chauvet, J.-L. Le Gouët and T. Chanelière, *Phys. Rev. Lett.* **120** (19), 197401 (2018).
27. F. Priolo, G. Franzò, S. Coffa, A. Polman, S. Libertino, R. Barklie and D. Carey, *J. Appl. Phys.* **78** (6), 3874-3882 (1995).
28. A. Terrasi, G. Franzò, S. Coffa, F. Priolo, F. D'Acapito and S. Mobilio, *Appl. Phys. Lett.* **70** (13), 1712-1714 (1997).
29. S. Probst, G. Zhang, M. Rancic, V. Ranjan, M. L. Dantec, Z. Zhong, B. Albanese, A. Doll, R. Liu and J. Morton, arXiv preprint arXiv:2001.04854 (2020).

This is the author's peer reviewed, accepted manuscript. However, the online version of record will be different from this version once it has been copyedited and typeset.

PLEASE CITE THIS ARTICLE AS DOI: 10.1063/1.50046904

30. W. B. Mims, *Phys.Rev.* **168** (2), 370-389 (1968).
31. R. A. Witte, *Electronic Test Instruments pg 201*. (Prentice Hall, 2002).
32. S. Welinski, P. J. Woodburn, N. Lauk, R. L. Cone, C. Simon, P. Goldner and C. W. Thiel, *Phys. Rev. Lett.* **122** (24), 247401 (2019).
33. A. M. Tyryshkin, S. Tojo, J. J. L. Morton, H. Riemann, N. V. Abrosimov, P. Becker, H.-J. Pohl, T. Schenkel, M. L. W. Thewalt, K. M. Itoh and S. A. Lyon, *Nat Mater* **11** (2), 143-147 (2012).
34. C. W. Thiel, N. Sinclair, W. Tittel and R. L. Cone, *Phys. Rev. B* **90** (21), 214301 (2014).
35. R. Rakhmatullin, I. Kurkin, G. Mamin, S. Orlinskii, M. Gafurov, E. Baibekov, B. Malkin, S. Gambarelli, S. Bertaina and B. Barbara, *Phys. Rev. B* **79** (17), 172408 (2009).

Supplementary Material

See the supplementary material for the TRIM simulation of the implant profile and details of the background echo subtraction.

Acknowledgements

This work was supported by the UK EPSRC grants EP/R011885/1 and EP/H026622/1. We acknowledge the European Research Council for financial support under the FP7 for the award of the ERC Advanced Investigator Grant SILAMPS 226470. We would like to thank Prof. John Morton for helpful discussions.

Data availability

The datasets generated during the current study are available in the Mendeley Data repository <http://dx.doi.org/10.17632/vt7vfm3jmb.1>

Competing financial interests: The authors declare no competing financial interest.

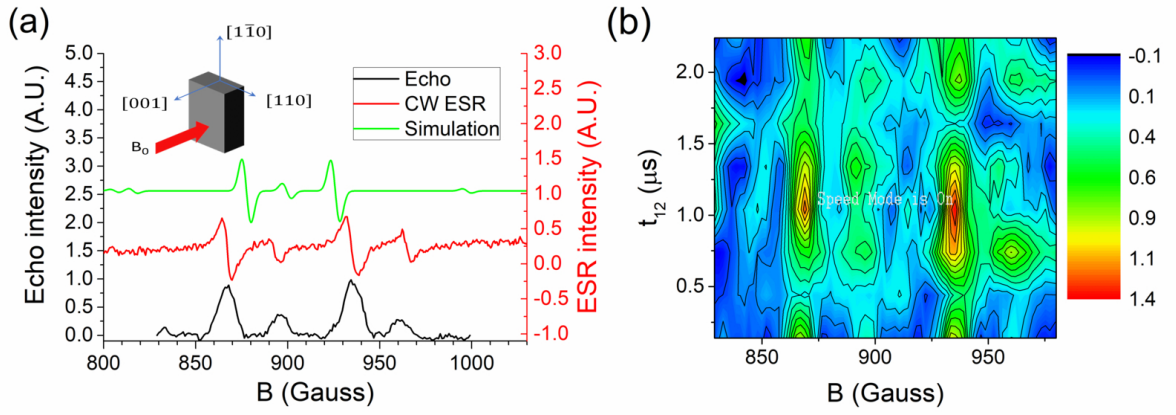
This is the author's peer reviewed, accepted manuscript. However, the online version of record will be different from this version once it has been copyedited and typeset.

PLEASE CITE THIS ARTICLE AS DOI: 10.1063/1.50046904

FIG 1 a) Simulated CW ESR of OEr-3 centre, measured CW ESR, and field dependent echo ($t_{12} = 130$ ns) signal. b) Contour plot showing the echo intensity as a function of magnetic field at various t_{12} . All CW ESR measurements were made at 10 K, all echo measurements at 5 K, and the microwave frequency was 9.61 GHz.

FIG 2 a) Spin echo decay profile at a B_0 of 867 G, with the off-resonance decay profile subtracted (black), fitted to Eq. 2 (red), with x fixed to 2 and fit parameters of $T_2 = 7.5 \pm 3$ μ s, $k = 0.46 \pm 0.1$, $\nu_L = 0.77 \pm 0.05$ MHz. Inset shows the saturation recovery at 867 G, with the off-resonance saturation recovery subtracted, (black) fitted with a single exponential fit (red) to give T_1 of 0.98 ± 0.2 ms. b) FFT of measured (black) and fitted (red) decay profiles; the position of the two main peaks in the FFT of the measured decay reveals two frequencies: $\nu_1 = 0.70$ MHz and $\nu_2 = 1.66$ MHz. All measurements were at 5 K, and the microwave frequency was 9.61 GHz.

This is the author's peer reviewed, accepted manuscript. However, the online version of record will be different from this version once it has been copyedited and typeset.
PLEASE CITE THIS ARTICLE AS DOI: 10.1063/5.0046904



This is the author's peer reviewed, accepted manuscript. However, the online version of record will be different from this version once it has been copyedited and typeset.
 PLEASE CITE THIS ARTICLE AS DOI: 10.1063/5.0046904

